CHAPTER ONE

Direct Electron Detectors

G. McMullan, A.R. Faruqi, R. Henderson[1]
MRC Laboratory of Molecular Biology, Cambridge, United Kingdom
[1]Corresponding author: e-mail address: rh15@mrc-lmb.cam.ac.uk

Contents

Abstract

Direct electron detectors have played a key role in the recent increase in the power of single-particle electron cryomicroscopy (cryoEM). In this chapter, we summarize the background to these recent developments, give a practical guide to their optimal use, and discuss future directions.

1. INTRODUCTION

Electron cryomicroscopy (cryoEM) has experienced a surge in its capability in recent years, due to improved microscopes, better detectors, and better software. The role of detectors has arguably been the central factor because it allowed the full benefit of many electron-optical improvements over the last decade to be exploited and has driven the development of new software to deal with the increased information content of the images.

Three companies produce the currently available direct electron detectors, Gatan, FEI, and Direct Electron. These are sometimes called Direct Detection Devices (DDD). In each case, the detectors produce images from 300 keV electrons that are significantly better than obtained with film (McMullan, Faruqi, Clare, & Henderson, 2014). All three products are based on similar sensor technology in which electrons directly impinge on a lightly doped silicon epilayer supported on a more highly doped silicon substrate,

Methods in Enzymology, Volume 579
ISSN 0076-6879
http://dx.doi.org/10.1016/bs.mie.2016.05.056

with each frame of the exposure being read out continuously in rolling-shutter mode as a "movie."

We present a brief history of how we reached this point, a methods section on the comparative merits of the new detectors and strategies for data collection, and conclude with a glimpse into the future to anticipate further developments.

2. PAST

Electronic image sensors developed over many years. The two technologies that have been most important in electron microscopy (EM) are charge-coupled devices (CCDs) and monolithic active pixel sensors (MAPSs) fabricated with standard complementary metal oxide semiconductor (CMOS) technology. Boyle and Smith from Bell Laboratories received the 2009 Nobel Prize in Physics for inventing the CCD sensor in 1969, which has had enormous success in light imaging. The name active pixel sensor (APS) was coined in 1985 by Nakamura and generalized by Fossum (1993) to describe any sensor with at least one active transistor within each pixel. In practice, at least two more transistors are required for row selection and reset. Fossum also pointed out that CMOS APSs allowed bigger arrays, faster readout, reduced noise, and reduced sensitivity to radiation damage compared with CCDs, and indeed CMOS sensors have eclipsed CCDs in most current applications where these advantages were critical. The onward march of Moore's law has reduced the size of lithography features in sensor manufacture. This has underpinned the evolution of better electronic image sensors and will continue to drive future developments.

Two parameters important in specifying the performance of detectors are Detective Quantum Efficiency (DQE) and Modulation Transfer Function (MTF). DQE, defined by

$$\mathrm{DQE} = (\mathrm{S/N})^2_{\mathrm{OUT}} / (\mathrm{S/N})^2_{\mathrm{IN}}$$

shows how much the noise or the physics of the mechanism of signal conversion in the detector degrades the original signal in the image, in terms of the signal-to-noise (S/N) ratio in the output compared with that in the input. DQE can be plotted as a function of spatial frequency and a DQE of unity implies a perfect detector adding no noise. For a pixelated detector, the pixel spacing fixes the maximum spatial frequency in an image that can be recorded by the detector, since the shortest wavelength must be sampled

at least twice. This sets the so-called Nyquist cut-off frequency as 1/(2*pixel_spacing). A representative value of DQE is often specified at half the maximum frequency, referred to as half Nyquist. The MTF specifies how strongly the various spatial frequencies in the image out to Nyquist are recorded and is set by the pixel size and other factors, such as the spreading of the electrons in the active layer of the detector. MTF is plotted as a function of spatial frequency and a value of unity implies perfect retention of the relative amplitude of that spatial frequency.

In EM, the introduction of electronic detectors in the 1990s as a replacement for photographic film (Krivanek & Mooney, 1993) was based on CCD sensors with a phosphor and fiber-optic coupling. The phosphor/fiber-optic, which converts the signal from a high-energy incident electron into a pulse of light photons, was essential because CCDs are easily destroyed by direct illumination with electrons. Their use for recording images or electron diffraction patterns (Downing & Hendrickson, 1999; Faruqi, Henderson, & Subramaniam, 1999) had both advantages and disadvantages. The advantage was that the microscopist could immediately see the quality of their specimen and thus avoid the long delay between exposure and observation of the image that occurred when using film. The disadvantage was that these early electronic cameras for EM were based on phosphor/fiber-optic/CCD technology, in which the DQE was only slightly better than that of film when used with 80 or 100 keV electrons. At higher voltages, although the microscope resolution, depth-of-focus, aberrations, and beam penetration improve, and the undesirable effects of beam-induced specimen charging are reduced, the DQE of these detectors was actually a lot worse than film. This was especially clear once techniques for measuring the frequency dependence of the DQE (De Ruijter, 1995; Meyer & Kirkland, 2000) were developed. Typically, the DQE of a phosphor/fiber-optic/CCD electron camera operated at 300 keV was 7–10% at half Nyquist resolution, much lower than film, which has a DQE at half Nyquist of 30–35% when using a 7 μm pixel size (McMullan, Chen, Henderson, & Faruqi, 2009). As a result, the highest-resolution single-particle structures determined prior to 2012 were largely obtained with images recorded on film (Grigorieff & Harrison, 2011; Zhang, Jin, Fang, Hui, & Zhou, 2010).

The reduced sensitivity to radiation damage of CMOS/MAPs compared with CCDs attracted the attention of the charged particle detection community beginning around 1998 (Caccia et al., 1999; Kleinfelder et al., 2002; Turchetta et al., 2001). The electron microscope community began to take note around 2003 (Evans et al., 2005; Faruqi et al., 2005; Milazzo et al., 2005; Turchetta, 2003; Xuong et al., 2004), and at this point in 2016,

it is fair to say that CMOS/MAPS technology is expected to dominate in TEM and probably in high-energy physics charged particle detection, such as at the Large Hadron Collider. Technical development of these CMOS/MAPS detectors was carried out between 2005 and 2010, with product announcements in 2009 and eventual delivery of the first commercial products in 2012.

3. PRESENT

CMOS/MAPS detectors have a rolling readout mechanism and mostly work with a rolling-shutter. They can read out images continuously with a frame rate that can range from 1 to 1000 Hz or more. The original designs for digital consumer cameras (Sunetra, Kemeny, & Fossum, 1993) were adapted for the detection of charged particles through some changes to the basic design of the pixels. The primary difference for the revised design was the inclusion of a thin p-epitaxial layer (Turchetta et al., 2001) above the substrate, shown schematically in Fig. 1A. The top surface consists of a passivation layer a few μm thick containing the electronics and interconnects for the readout. Fig. 1B shows an example of one type of pixel design with three transistors (3T) in the readout electronics. This design is the simplest type of active pixel and is still popular; however, there are a number of more complex designs with additional transistors, which can provide some advantages, such as reducing the readout noise by correlated double sampling of the pixel charge.

The basic operation of this 3T pixel geometry is as follows (Mendis et al., 1997). Part of the energy of the incoming primary electron is converted into electron–hole pairs in the epilayer, which has a typical thickness of 5–20 μm. Due to doping differences in p − and p + silicon there is a potential barrier at the boundary between the epilayer and the substrate on one side and the P-wells on the other side. This means that radiation-generated electrons are kept within the epilayer and eventually will be collected by the N-well diode through a mixture of drift and diffusion processes. Prior to starting an exposure in each frame, transistor T1 resets the diode capacitance by charging it up to the reset voltage, which is usually between 1 and 3 V. The collected charge from the electron/hole pairs that are created by the electric field of the high-energy incident electrons then discharges the capacitance on the input of T1 (Fig. 1B) and constitutes the signal (Prydderch et al., 2003). The T1/diode reset also introduces unwanted kTC noise to the collection node voltage. kTC noise refers to the variation

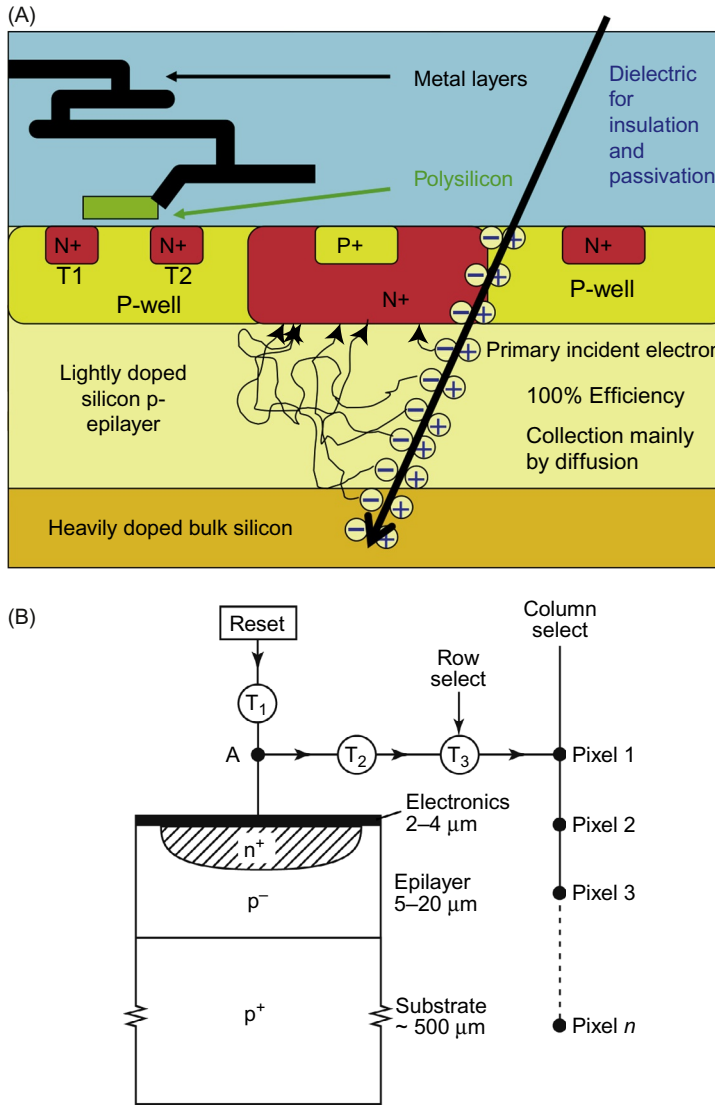

Fig. 1 (A) Schematic diagram viewed parallel to the sensor surface, of a single pixel in a typical CMOS sensor. The incident electron is represented by the *black arrow* from *top right* to *bottom left*. The + and − symbols indicate the electron–hole pairs that are created by the transient electric field as the high-energy electron passes. The mini-electrons are collected by the N-well whose potential drops during the exposure. (B) Schematic of readout for a single pixel, showing the 3T logic and its relationship to the N+ diode/capacitor. *Panel (A): Adapted from Turchetta, R. (2003). CMOS monolithic active pixel sensors (MAPS) for scientific applications. In:* 9th Workshop on electronics for LHC experiments Amsterdam, 2003 *(pp. 1–6).* http://lhc-electronics-workshop.web.cern.ch/lhc-electronics-workshop/2003/PLENARYT/TURCHETT.PDF. *Panel (B): Reproduced from Faruqi, A. R. (2007). Direct electron detectors for electron microscopy.* Advances in Imaging and Electron Physics, 145*, 55–93.*

in the reset voltage due to thermal fluctuations in the charge on the capacitance of the diode. It is possible to reduce the effects of kTC noise by reading out twice: once immediately after reset and once after arrival of the signal followed by subtraction of the first value from the second; this is called correlated double sampling (CDS). On readout after the exposure, transistor T2 acts as source follower transferring the voltage signal to the readout transistor T3. The charge is read out by selecting rows (by activating T3) and reading out the corresponding pixels in all the columns, repeating the process for all rows. The reduction in diode voltage, proportional to charge collected on each pixel, is digitized either by on-chip or external analog-to-digital converters (ADCs), then corrected for systematic differences in pixel sensitivity by bright-field and dark-field calibrations, before being formed into an image that is used for further analysis.

Fig. 2A shows a typical layout of the pixels in a 4k × 4k sensor. Fig. 2B shows how several of these sensors are manufactured on a typical 200 mm wafer, before being diced, backthinned, mounted, and bonded. Finally, the fully mounted sensor is housed in an evacuated camera chamber, which requires electrical feedthroughs, cooling to reduce electronic noise, and possibly a mechanism for retraction if the microscope is used in other modes or with other detectors.

The frame readout rate depends on how many ADCs are used simultaneously to digitize the voltages from the diodes. The effect of radiation damage on the detector can be minimized both by using special radiation-hard design features, but also by increasing the frame rate, since the main effect of radiation damage is to increase the leakage current, which discharges the diode capacitance even in the absence of illumination, and this is less important at fast frame rates. Backthinning can be used to make the sensors very thin (~30 μm) and this reduces the noise contribution from backscattered electrons (Fig. 3). The MTF and DQE of a direct electron detector can be improved by a factor of 2 or more by backthinning (McMullan, Faruqi, et al., 2009). The reduction of backscattering also results in a two- to threefold improvement in detector lifetime due to reduced overall energy deposition in the sensitive layer.

The new detectors can operate in either integrating mode or counting mode. In integrating mode, the amount of energy deposited in each pixel is read out directly as an analog voltage that is digitized and represents the image after dark-field and bright-field corrections. Because the interaction of each high-energy electron with the sensor is stochastic, as illustrated in Fig. 3, the amount of energy deposited by each incident electron can vary

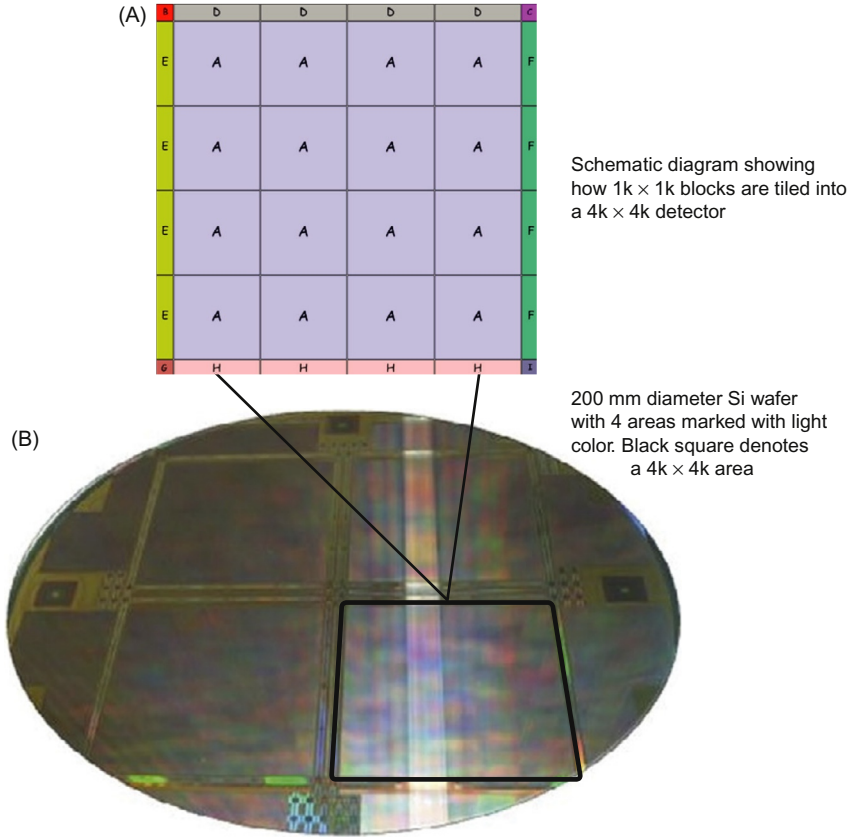

Fig. 2 (A) Typical layout of a stitched sensor with 4096 × 4096 pixels. Block A consists of a 1024 × 1024 pixel array that is tiled four times in each direction, but the number of blocks can be increased to produce larger area detectors. The edge blocks B through I control the addressing, reset and readout. (B) 200 mm silicon wafer showing the arrangement of four detectors. *Adapted from Guerrini, N., Turchetta, R., Van Hoften, G., Henderson, R., McMullan, G., & Faruqi, A. R. (2011). A high frame rate, 16 million pixels, radiation hard CMOS sensor.* Journal of Instrumentation, 6 C03003.

by a factor of 40 or more. This limits the DQE to about 60%, though parameter choice during design and manufacture, such as use of a thin epilayer and small pixels, can make this much lower. In counting mode, the intensity of the illumination is reduced by a factor of several hundred to a dose rate of perhaps only one electron per 100 pixels per frame. Individual electron events are then identified and replaced computationally by a delta function or a more sophisticated function (Li, Mooney, et al., 2013; McMullan, Clark, Turchetta, & Faruqi, 2009; Turchetta, 1993), so that each event gets

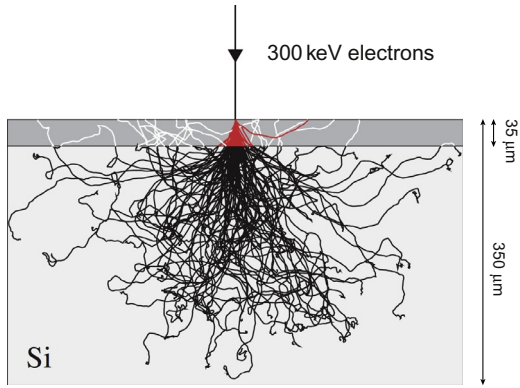

Fig. 3 Schematic of 300 keV electron trajectories, showing a Monte Carlo simulation of 300 keV electron tracks in silicon. After backthinning to 35 µm, only those parts of the electron tracks highlighted in *red* would contribute to the recorded signal. Before backthinning, the additional *white tracks* would contribute a low-resolution component to the signal together with contributions to the noise at all spatial frequencies. The overall thickness of the silicon in the figure is 350 µm with the 35 µm layer that remains after backthinning shown in *gray*. *Reproduced from McMullan, G., Faruqi, A. R., Henderson, R., Guerrini, N., Turchetta, R., Jacobs, A., & van Hoften, G. (2009). Experimental observation of the improvement in MTF from backthinning a CMOS direct electron detector.* Ultramicroscopy, 109*(9), 1144–1147.*

the same weight. In principle, if the signal-to-noise ratio for each event is high enough and its location can be determined accurately enough, this can give much higher DQE(0) and DQE(Nyquist), respectively.

The currently available direct electron detectors are the K2 from Gatan, recently upgraded to K2-XP, the Falcon II from FEI, recently upgraded to Falcon III, and DE-20 from Direct Electron, with a recent addition of DE-64. In each case, their detectors produce images using 300 keV electrons that are significantly better than obtained with film (Fig. 4 and McMullan et al., 2014). The DQE at half the Nyquist frequency is in the range 40–60% for the detectors when used in integrating mode, but typically drops to ~25% at the Nyquist frequency. Higher DQE values than these can only be obtained by operating in counting mode where the image of each incident electron is substituted by an idealized single count, so all future improved detectors will need to operate in counting mode. Higher frame rates are also required for counting, to avoid either double hits on individual pixels or very long exposures times, and at present only the Gatan K2, when operated in counting mode, can produce a DQE(0) as high as 80% in conjunction with reasonably small exposure times (Li, Mooney, et al., 2013;

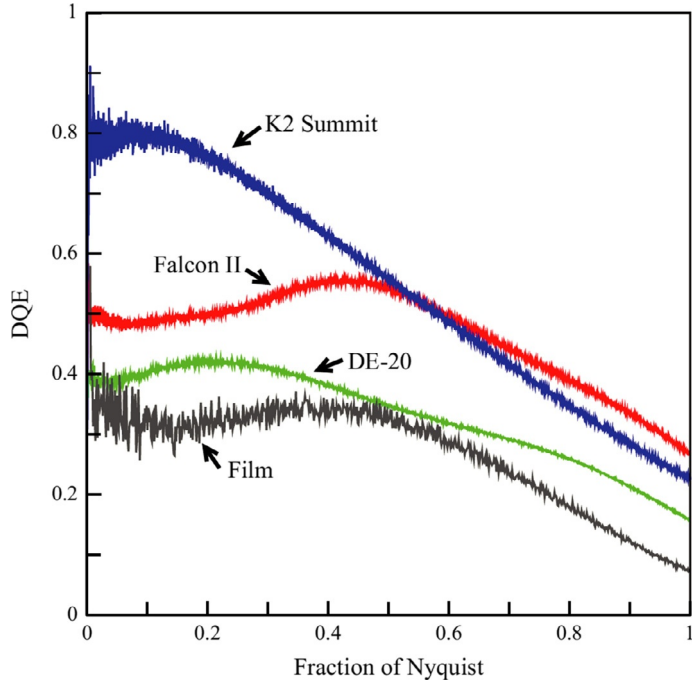

Fig. 4 Comparison of DQE at 300 keV as a function of spatial frequency for the DE-20 (*green* (*light gray* in the print version)), Falcon II (*red* (*gray* in the print version)), and K2 Summit (*blue* (*dark gray* in the print version)). The corresponding DQE of photographic film is shown in *black. Reproduced from McMullan, G., Faruqi, A. R., Clare, D., & Henderson, R. (2014). Comparison of optimal performance at 300 keV of three direct electron detectors for use in low dose electron microscopy.* Ultramicroscopy, 147*, 156–163.*

Li, Zheng, Egami, Agard, & Cheng, 2013). The K2 detector frame rate is about 10 times higher than that available with the two other detector brands. If the arrival point of each incident electron can be determined to subpixel accuracy with sufficient precision, there is no reason why the DQE(ω) should not approach 100% without much drop at Nyquist, and the detectors might then be usable beyond Nyquist in super-resolution mode. The K2 detector already allows operation in super-resolution mode, but has relatively low DQE(Nyquist). An increased DQE at and beyond Nyquist would make it and other detectors that can operate in the counting mode much more powerful. FEI and Direct Electron have both announced that the Falcon and DE can be run in counting mode, producing higher DQE but at the expense of longer exposure times. It is too early to see whether practical data collection is viable.

The improved DQE of the new direct electron detectors, together with the ability to record high frame rate movies, has brought synergistic advantages. The improved DQE alone provides a big gain in the signal-to-noise ratio in this recorded image. The availability of movie recording allows the effect of beam-induced specimen movement and image blurring to be reduced by subsequent alignment and appropriate weighting of the individual frames, thus increasing the sharpness of the particle images (Bai, Fernandez, McMullan, & Scheres, 2013; Brilot et al., 2012; Campbell et al., 2012; Grant & Grigorieff, 2015; Li, Mooney, et al., 2013; Ripstein & Rubinstein, 2016; Rubinstein & Brubaker, 2015; Scheres, 2014; Vinothkumar, McMullan, & Henderson, 2014). An example of this is shown in Fig. 5, and another example can be seen in Brilot et al. (2012). These improved motion-corrected images then allow the more accurate determination of the position and orientation of each particle, which produces a 3D map of the structure at higher resolution than it would be without the corrections applied. This higher resolution map then provides a better target for the orientation determination in an iterative manner. Thus the new generation of detectors has produced a bigger impact on the attainable resolution than might have been expected from the increased DQE alone.

The improvement in DQE that is possible by electron counting is most apparent presently at low resolution on the K2 detector (Fig. 4). This improvement can be exploited by recording images at higher magnification than might normally be chosen, for example, at 0.7 or 1.0 Å per pixel, and by carrying out subsequent 2×2 or 3×3 binning. We now discuss briefly the practical choice of parameters for cryoEM illumination conditions to optimize image quality for each of the new detectors.

3.1 Practical Advice for the User

This paragraph may be the most useful for the user who simply wants to know what settings to use to get the most out of the new detectors. Typical microscope parameters used for acquisition of high-resolution images and movies with the three detector types are given in Table 1, and are discussed in more detail by Passmore and Russo (2016). Briefly, each detector has an optimum dose rate at which the DQE is maximal. At higher doses, the detectors all saturate so that each frame of the movie would then effectively contain no information. Likewise, at very low dose rates, many frames have to be added together to give an image with adequate total exposure and these

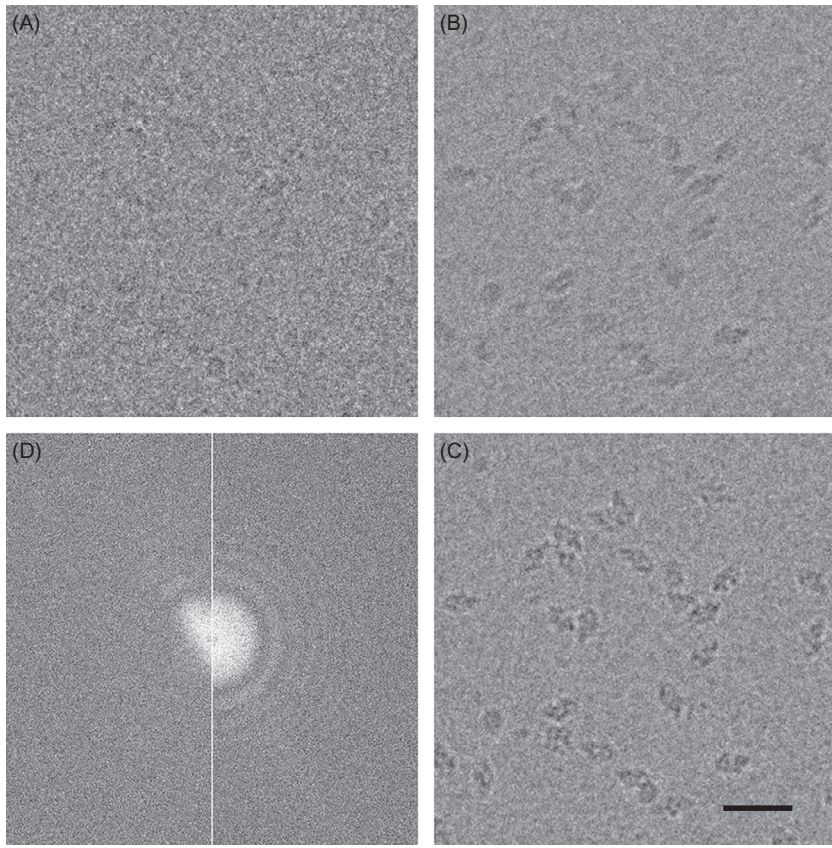

Fig. 5 Image of a 1024 × 1024 pixel area of a cryoEM image (20.21.43) of a typical structural biology specimen of the *E. coli* enzyme β-galactosidase, showing (A) single frame with an electron dose of ~6 electrons/Å^2, the sum of movie frames with a total electron dose of ~50 electrons/Å^2 without (B) and with (C) alignment, and (D) the power spectra (Fourier transforms) of the unaligned (*left*) and aligned (*right*) images out to half Nyquist (1/7 Å^{-1}). The images were recorded at 300 keV on an FEI Krios microscope with a Falcon II detector using 1.75 Å pixel size and ~3.5 μm defocus. Scale bar 300 Å.

summed images would then be dominated by electronic readout noise. In practice, the DQE versus dose rate curve is fairly broad, so a range of exposures is acceptable. For the Falcon II detector the range from 0.2 to 4.5 electrons/pixel/frame is usable (Kuijper et al., 2015). For DE, the range from 0.15 to 3.0 is viable. For K2 Summit, the range from 0.002 to 0.025 electrons/pixel/400 Hz frame is reasonable (Li, Mooney, et al., 2013; Li, Zheng, et al., 2013). For typical magnification choices, this translates into 15–40 electrons/Å^2/s for Falcon and DE, or 1–8 electrons/Å^2/s for K2.

Table 1 Typical Microscope Parameters Used for Acquisition of High-Resolution Images and Movies with the Three Detector Types

Camera	Direct Electron DE-20 (Integrating Mode)	FEI Falcon II (Integrating Mode)	Gatan K2 Summit (Counting Mode)
Pixel size at detector (μm)	6.4	14	5
Pixel size at specimen (Å)	1.0–1.3	1.7	1.0–1.4
Magnification (detector/specimen)	50–60 k ×	80 k ×	35–50 k ×
Movie frames/s (Hz)	20–32	17	400
Electron dose at detector (electrons/pixel/frame)	1.4–2	3	0.012–0.02
Electron dose at specimen (electrons/Å^2/s)	24–38	17	2.5–8
Total exposure time (seconds)	1.5–3.0	3	6–16
Total electron exposure (electrons/Å^2)	52–75	51	40–48

The saturating dose rate is several hundred times higher when the detector is used in integrating mode compared with counting mode, so both the Falcon and DE detectors can be operated as integrating detectors at dose rates up to 2 or 3 electrons/pixel/frame, whereas the dose rate in counting mode should be kept below 0.01–0.025 electrons/pixel/frame. In practice, this means the total exposure time for Falcon and DE is in the range 1–3 s, whereas with the K2, exposures are normally in the range of 6–16 s, or even longer if a bigger pixel size is used, as shown in Table 1. This means that the Falcon and DE detectors can easily be used on microscopes that have less stable cold stages with significant stage drift. In comparison, the K2 detector with its thin epilayer has a relatively poor DQE when operated in integrating mode, so in practice the K2 should always be used in counting mode (either with or without super-resolution, subpixel interpolation). Conversely, the exposure times for Falcon and DE detectors in counting mode would be very long, possibly more than 60 s, so at this moment there is no published structural determination using these detectors in counting mode.

4. FUTURE

Further improvements in detector performance require solving one or two remaining problems. First it is important that detectors should be developed so that their DQE is closer to 100%. This will require universal adoption of electron counting since the distribution of energy deposition when individual electrons pass through any detector is stochastic (Fig. 6) and the so-called Landau distribution (Fig. 7) of energy deposited by individual electron events has a very wide spread. Electron counting can be done on any of the CMOS detectors but is too slow for normal use unless the frame rate is high. A reasonably high frame rate is already available commercially with the Gatan K2/Summit detector (Li, Mooney, et al., 2013; Li, Zheng, et al., 2013), and a paper describing the counting mode of the FEI Falcon III camera was recently published (Kuijper et al., 2015). Any implementation of electron counting will benefit from minimizing missed or overlapping events, which requires a high signal-to-noise ratio and a high frame rate.

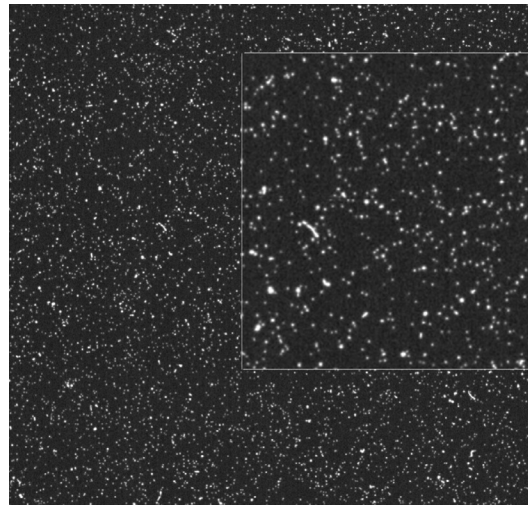

Fig. 6 Single frame image recorded using 300 keV electrons, showing single electron events on an FEI Falcon III detector, with excellent signal-to-noise ratio. A magnified portion is inset. Falcon III is a highly backthinned sensor with very low noise level. The single frame shows about 100,000 electron events (ie, one electron per 150 pixels). *This figure is similar to that for Falcon III in Kuijper, M., van Hoften, G., Janssen, B., Geurink, R., De Carlo, S., Vos, M., … Storms, M. (2015). FEI's direct electron detector developments: Embarking on a revolution in cryo-TEM.* Journal of Structural Biology, 192*(2), 179–187.*

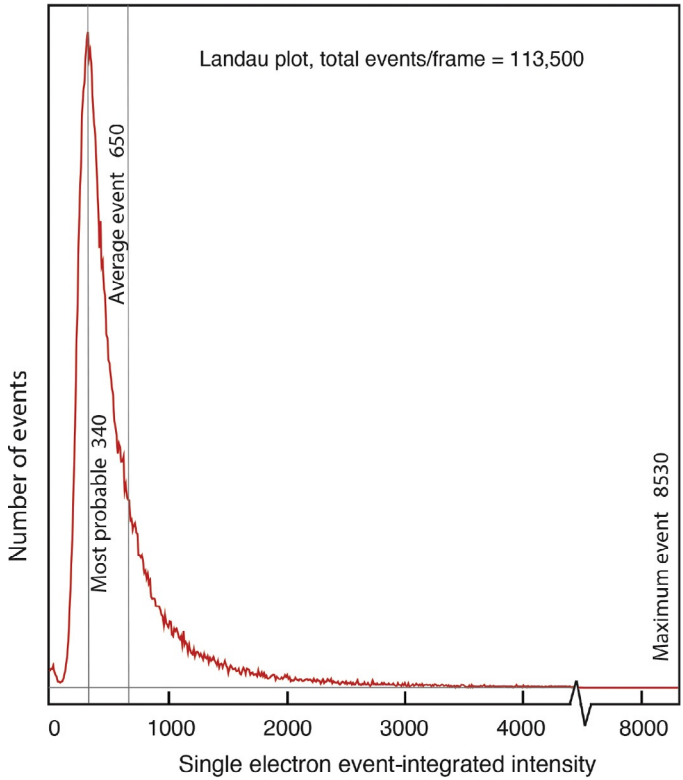

Fig. 7 Landau intensity distribution for the single electron events from the image shown in Fig. 6. Single electron events are identified by an initial threshold criterion and then all pixels contributing to each event are added together to determine the total signal from each electron. The Landau plot is the histogram of the single electron event distribution.

Improving the signal-to-noise ratio of the readout helps to minimize missed events. A larger pixel size would allow the use of a thicker epilayer with a resulting increased signal; a greater degree of backthinning reduces the incidence of extended electron tracks. Accurate subpixel localisation is incompatible with events that appear as tracks. However, although it may be possible to get DQE(0) to approach 100%, it is unrealistic to expect DQE(Nyquist) to exceed 80–90%, since this would require the accuracy of subpixel localization of electron events to be better than ± 0.15 pixels. A very small number of electrons will always be backscattered elastically from the detector surface without depositing any energy. Others may pass through and deposit very little energy so they may remain undetected, unless

the epilayer is thick enough to improve signal-to-noise ratio. Others will be scattered sideways (Fig. 3) to leave tracks of deposited energy that contain no high-resolution information. Finally, unless the frame rate is very high there will always be the temptation to increase the beam intensity, thus increasing the number of overlapping events and reducing the overall DQE.

The technology used for direct electron detectors is very similar to that used in digital cameras and phones. The feature sizes used in sensor lithography have dropped from around 1 μm in the early 1990s to 65 nm in some of the latest mobile phone cameras in 2016. In corresponding state-of-the-art central processor units, feature sizes as small as 14 nm are being used. The current EM sensors use 350 nm or 180 nm technology that is years behind the industry leaders. With reasonable further investment in direct electron detector development, it is possible to envisage bigger, faster, electron counting sensors that would further revolutionize the speed and quality of image recording. We can certainly look forward to being able to tackle even more challenging biological structures, whether using single particle or tomography approaches, to determine smaller (and larger) structures using fewer images to higher resolution and with the ability to distinguish more three-dimensional states than at present. The future holds great promise.

REFERENCES

Bai, X. C., Fernandez, I. S., McMullan, G., & Scheres, S. H. W. (2013). Ribosome structures to near-atomic resolution from thirty thousand cryo-EM particles. *eLife*, *2*, e00461.

Brilot, A. F., Chen, J. Z., Cheng, A. C., Pan, J. H., Harrison, S. C., Potter, C. S., … Grigorieff, N. (2012). Beam-induced motion of vitrified specimen on holey carbon film. *Journal of Structural Biology*, *177*(3), 630–637.

Caccia, M., Campagnolo, R., Meroni, C., Kucewicz, W., Deptuch, G., Zalewska, A., … Turchetta, R. (1999). *High resolution pixel detectors for e+e- linear colliders.* arXiv:hep-ex/9910019v1.

Campbell, M. G., Cheng, A. C., Brilot, A. F., Moeller, A., Lyumkis, D., Veesler, D., … Grigorieff, N. (2012). Movies of ice-embedded particles enhance resolution in electron cryo-microscopy. *Structure*, *20*(11), 1823–1828.

De Ruijter, W. J. (1995). Imaging properties and applications of slow-scan charge-coupled-device cameras suitable for electron-microscopy. *Micron*, *26*(3), 247–275.

Downing, K. H., & Hendrickson, F. M. (1999). Performance of a 2 k CCD camera designed for electron crystallography at 400 kV. *Ultramicroscopy*, *75*(4), 215–233.

Evans, D. A., Allport, P. P., Casse, G., Faruqi, A. R., Gallop, B., Henderson, R., … Waltham, N. (2005). CMOS active pixel sensors for ionising radiation. *Nuclear Instruments & Methods in Physics Research Section A—Accelerators, Spectrometers, Detectors and Associated Equipment*, *546*(1–2), 281–285.

Faruqi, A. R., Henderson, R., Pryddetch, M., Allport, P., Evans, A., & Turchetta, R. (2005). Direct single electron detection with a CMOS detector for electron microscopy. *Nuclear Instruments & Methods in Physics Research Section A—Accelerators, Spectrometers, Detectors and Associated Equipment*, *546*(1–2), 170–175.

Faruqi, A. R., Henderson, R., & Subramaniam, S. (1999). Cooled CCD detector with tapered fibre optics for recording electron diffraction patterns. *Ultramicroscopy*, *75*(4), 235–250.

Fossum, E. R. (1993). Active pixel sensors—Are CCDs dinosaurs. In *Charge-coupled devices and solid state optical sensors III: Vol. 1900*. (pp. 2–14). http://dx.doi.org/10.1117/12.148585.

Grant, T., & Grigorieff, N. (2015). Measuring the optimal exposure for single particle cryo-EM using a 2.6 Å reconstruction of rotavirus VP6. *eLife*, *4*, e06980. http://dx.doi.org/10.7554/eLife.06980.

Grigorieff, N., & Harrison, S. C. (2011). Near-atomic resolution reconstructions of icosahedral viruses from electron cryo-microscopy. *Current Opinion in Structural Biology*, *21*(2), 265–273.

Kleinfelder, S., Bichsel, H., Bieser, F., Matis, H. S., Rai, G., Retiere, F., … Yamamoto, E. (2002). Integrated X-ray and charged particle active pixel CMOS sensor arrays using an epitaxial silicon sensitive region. *Proceedings of SPIE*, *4784*, 208–217. http://dx.doi.org/10.1117/12.450826.

Krivanek, O. L., & Mooney, P. E. (1993). Applications of slow-scan CCD cameras in transmission electron-microscopy. *Ultramicroscopy*, *49*(1–4), 95–108.

Kuijper, M., van Hoften, G., Janssen, B., Geurink, R., De Carlo, S., Vos, M., … Storms, M. (2015). FEI's direct electron detector developments: Embarking on a revolution in cryo-TEM. *Journal of Structural Biology*, *192*(2), 179–187.

Li, X. M., Mooney, P., Zheng, S., Booth, C. R., Braunfeld, M. B., Gubbens, S., … Cheng, Y. F. (2013). Electron counting and beam-induced motion correction enable near-atomic-resolution single-particle cryo-EM. *Nature Methods*, *10*(6), 584–590.

Li, X. M., Zheng, S. Q., Egami, K., Agard, D. A., & Cheng, Y. F. (2013). Influence of electron dose rate on electron counting images recorded with the K2 camera. *Journal of Structural Biology*, *184*(2), 251–260.

McMullan, G., Chen, S., Henderson, R., & Faruqi, A. R. (2009). Detective quantum efficiency of electron area detectors in electron microscopy. *Ultramicroscopy*, *109*(9), 1126–1143.

McMullan, G., Clark, A. T., Turchetta, R., & Faruqi, A. R. (2009). Enhanced imaging in low dose electron microscopy using electron counting. *Ultramicroscopy*, *109*(12), 1411–1416.

McMullan, G., Faruqi, A. R., Clare, D., & Henderson, R. (2014). Comparison of optimal performance at 300 keV of three direct electron detectors for use in low dose electron microscopy. *Ultramicroscopy*, *147*, 156–163.

McMullan, G., Faruqi, A. R., Henderson, R., Guerrini, N., Turchetta, R., Jacobs, A., & van Hoften, G. (2009). Experimental observation of the improvement in MTF from back-thinning a CMOS direct electron detector. *Ultramicroscopy*, *109*(9), 1144–1147.

Mendis, S. K., Kemeny, S. E., Gee, R. C., Pain, B., Staller, C. O., Kim, Q. S., & Fossum, E. R. (1997). CMOS active pixel image sensors for highly integrated imaging systems. *IEEE Journal of Solid-State Circuits*, *32*(2), 187–197. http://dx.doi.org/10.1109/4.551910.

Meyer, R. R., & Kirkland, A. I. (2000). Characterisation of the signal and noise transfer of CCD cameras for electron detection. *Microscopy Research and Technique*, *49*(3), 269–280.

Milazzo, A. C., Leblanc, P., Duttweiler, F., Jin, L., Bouwer, J. C., Peltier, S., … Xuong, N. H. (2005). Active pixel sensor array as a detector for electron microscopy. *Ultramicroscopy*, *104*(2), 152–159.

Passmore, L. A., & Russo, C. J. (2016). Specimen preparation for high-resolution cryo-EM. *Methods in Enzymology*, *579*, 51–86.

Prydderch, M. L., Waltham, N. J., Turchetta, R., French, M. J., Holt, R., Marshall, A., … Mapson-Menard, H. (2003). A 512 x 512 CMOS monolithic active pixel sensor with

integrated ADCs for space science. *Nuclear Instruments & Methods in Physics Research Section A—Accelerators, Spectrometers, Detectors and Associated Equipment*, *512*(1–2), 358–367. http://dx.doi.org/10.1016/S0168-9002(03)01914-4.

Ripstein, Z. A., & Rubinstein, J. L. (2016). Processing of cryo-EM movie data. *Methods in Enzymology*, *579*, 103–124.

Rubinstein, J. L., & Brubaker, M. A. (2015). Alignment of cryo-EM movies of individual particles by optimization of image translations. *Journal of Structural Biology*, *192*(2), 188–195.

Scheres, S. H. W. (2014). Beam-induced motion correction for sub-megadalton cryo-EM particles. *eLife*, *3*, e03665.

Sunetra, K. M., Kemeny, S. E., & Fossum, E. R. (1993). A 128x128 CMOS active pixel image sensor for highly integrated imaging systems. In *IEEE, IEDM'93* (pp. 583–586). http://dx.doi.org/10.1109/IEDM.1993.347235.

Turchetta, R. (1993). Spatial-resolution of silicon microstrip detectors. *Nuclear Instruments & Methods in Physics Research Section A—Accelerators, Spectrometers, Detectors and Associated Equipment*, *335*(1–2), 44–58.

Turchetta, R. (2003). CMOS monolithic active pixel sensors (MAPS) for scientific applications. In *9th Workshop on electronics for LHC experiments, Amsterdam, 2003* (pp. 1–6). http://lhc-electronics-workshop.web.cern.ch/lhc-electronics-workshop/2003/PLENARYT/TURCHETT.PDF.

Turchetta, R., Berst, J. D., Casadei, B., Claus, G., Colledani, C., Dulinski, W.,Winter, M. … (2001). A monolithic active pixel sensor for charged particle tracking and imaging using standard VLSI CMOS technology. *Nuclear Instruments & Methods in Physics Research Section A—Accelerators, Spectrometers, Detectors and Associated Equipment*, *458*(3), 677–689. http://dx.doi.org/10.1016/S0168-9002(00)00893-7.

Vinothkumar, K. R., McMullan, G., & Henderson, R. (2014). Molecular mechanism of antibody-mediated activation of beta-galactosidase. *Structure*, *22*(4), 621–627.

Xuong, N. H., Milazzo, A. C., LeBlanc, P., Duttweiler, F., Bouwer, J., Peltier, S., … Kleinfelder, S. (2004). First use of a high sensitivity active pixel sensor array as a detector for electron microscopy. *Proceedings of SPIE*, *5301*, 242–249. http://dx.doi.org/10.1117/12.526021.

Zhang, X., Jin, L., Fang, Q., Hui, W. H., & Zhou, Z. H. (2010). 3.3 angstrom cryo-EM structure of a nonenveloped virus reveals a priming mechanism for cell entry. *Cell*, *141*(3), 472–482.